A 12-Million-Year Temperature History of the Tropical Pacific Ocean

Yi Ge Zhang *et al.*

Science **344**, 84 (2014);
DOI: 10.1126/science.1246172

A 12-Million-Year Temperature History of the Tropical Pacific Ocean

Yi Ge Zhang,[1]* Mark Pagani,[1] Zhonghui Liu[2]

The appearance of permanent El Niño–like conditions prior to 3 million years ago is founded on sea-surface temperature (SST) reconstructions that show invariant Pacific warm pool temperatures and negligible equatorial zonal temperature gradients. However, only a few SST records are available, and these are potentially compromised by changes in seawater chemistry, diagenesis, and calibration limitations. For this study, we establish new biomarker-SST records and show that the Pacific warm pool was ~4°C warmer 12 million years ago. Both the warm pool and cold tongue slowly cooled toward modern conditions while maintaining a zonal temperature gradient of ~3°C in the late Miocene, which increased during the Plio-Pleistocene. Our results contrast with previous temperature reconstructions that support the supposition of a permanent El Niño–like state.

Temperatures of the low-latitude Pacific Ocean substantially influence regional and global climates. In particular, the El Niño–Southern Oscillation (ENSO) dominates Earth's interannual climate variability. El Niño is initiated by the eastward propagation of warm western Pacific equatorial waters that deepen thermocline depths and attenuate upwelling rates across the eastern equatorial Pacific (EEP) (*1*, *2*). Regional sea-surface temperature (SST) change associated with El Niño affects the position and vigor of the Walker circulation and Hadley cell, leading to substantially reduced equatorial SST gradients, higher global mean temperatures, extratropical heat export, and regional hydrological impacts (*1*, *2*).

The western equatorial Pacific warm pool is among the warmest surface water on Earth, whereas the EEP, known as the cold tongue, is characterized by cold, nutrient-rich waters that result from a shallow thermocline and intense upwelling rates. The modern SST gradient between the warm pool and cold tongue averages 4° to 5°C (*3*) and varies in response to ENSO. Accordingly, paleo-SST reconstructions from these regions and the resulting character of the east-west temperature gradient have been used to describe broad climate states over the past 5 million years, particularly during the Pliocene epoch [5.3 to 2.6 million years ago (Ma)], when atmospheric CO_2 concentrations appear similar to today (*4*, *5*) and global temperatures are simulated to be 3° to 4°C warmer than preindustrial conditions (*6*, *7*).

Published temperature records based on magnesium-to-calcium ratios (Mg/Ca) of the planktonic foraminifera *Globoritalia sacculifer*, from Ocean Drilling Program (ODP) site 806 (0°N, 159°E) (Fig. 1) (*8*), suggest that warm pool temperatures remained relatively constant as Earth cooled over the past 5 million years. Curiously, existing Mg/Ca-based SST records also indicate that the Pacific warm pool of the Pliocene warm period (4.5 to 3 Ma) was ~0.5°C colder than the mean temperature of the late Quaternary (1.5 to 0 Ma), implying that warm pool temperatures were cooler or invariant during periods of global warmth. The appearance of invariant tropical temperatures during periods of global warmth implies a "tropical thermostat" (*9*) in which tropical warming is limited through evaporation or cloud feedbacks irrespective of the greenhouse gas forcing. However, this phenomenon is not supported by climate simulations (*10*), and much warmer tropical SSTs are evident during "super greenhouse" climate states in Earth history (e.g., the Cretaceous) (*11*).

In contrast to the western Pacific warm pool, temperature records from the eastern Pacific sites 847 (0°N, 95°W; based on Mg/Ca and the alkenone unsaturation index $U^{K'}_{37}$) (*8*, *12*) and 846 (3°S, 91°W; based on $U^{K'}_{37}$) (*13*) exhibit cooling for the past 5 million years. Consequently, warm pool and cold tongue SSTs result in a negligible equatorial temperature gradient during the early Pliocene (*8*, *14*) similar to those expressed during brief modern El Niño events (*8*, *14*). A nearly absent equatorial temperature gradient is argued to reflect a permanent El Niño–like state prior to 3 million years ago and has been further interpreted to reflect the establishment of a deep thermocline in the EEP, substantially reduced cold-water upwelling (*14*), an attenuated Walker circulation (*7*), and negligible ENSO variability (*14*). In contrast, high-resolution, coral $\delta^{18}O$ records (*15*) and isotope records of individual planktonic foraminifera from site 846 (*16*) indicate that the frequency and intensity of Pliocene ENSO-like oscillations were similar to those of today.

The veracity of the permanent El Niño supposition rests on the accuracy of paleotemperature reconstructions. In particular, *G. sacculifer* Mg/Ca-based SST records used to infer invariant warm pool SSTs assume that foraminifera Mg/Ca compositions are uninfluenced by diagenetic alteration or temporal changes in seawater chemistry [e.g., seawater Mg/Ca ratio (Mg/Ca_{sw})] and/or carbonate ion effect; see supplementary materials). However, $\delta^{18}O$ records on the identical samples (*8*) fail to capture the modern SST gradient (supplementary materials) and suggest the contribution of diagenetic carbonates. In addition, changes in Mg/Ca_{sw} could have lowered Pliocene

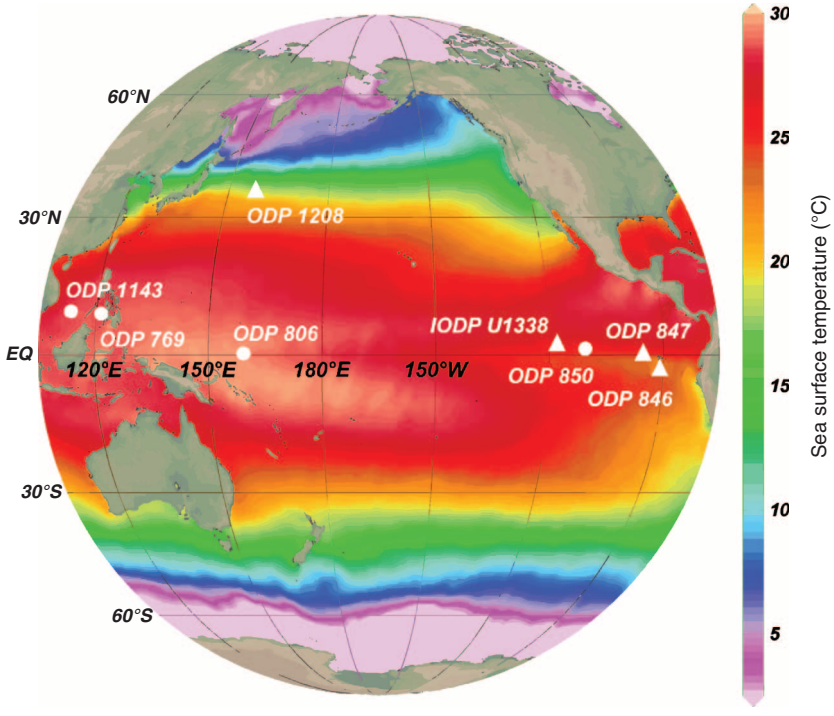

Fig. 1. Pacific sites discussed in this study. Colors represent modern mean annual SSTs. Circles represent sites analyzed in this study: ODP sites 769, 806, 850, and 1143. Triangles represent sites with previously published SSTs: ODP sites 846, 847, and 1208 (36°N, 128°E) and Integrated Ocean Drilling Program (IODP) site U1338 (3°N, 118°W). Map generated by Ocean Data View.

[1]Department of Geology and Geophysics, Yale University, New Haven, CT 06511, USA. [2]Department of Earth Sciences, The University of Hong Kong, Hong Kong SAR, China.

*Corresponding author. E-mail: yige.zhang@yale.edu

SST estimates because fluid inclusion (*17*) and carbonate veins (*18*) data indicate lower Mg/Ca_{sw} during the Pliocene. Notably, other warm pool temperature records derived from $U^{K'}_{37}$ values (*19*) are limited by the nature of the temperature proxy itself, which reaches a maximum calculable SST value of ~28.5°C (*20*) and thus compromises its capacity to record even higher SSTs (supplementary materials).

In summary, given possible diagenetic overprinting, seawater chemistry changes, and calibration limitations, available SST records likely underestimate maximum warm pool temperatures and potentially distort zonal SST gradient estimates.

For this study, we established new equatorial Pacific SST records using the TEX_{86} temperature proxy. TEX_{86} thermometry is founded on the distribution of the archaeal lipid membranes, glycerol dialkyl glycerol tetraethers, primarily produced by archaea from the phylum *Thaumarchaeota*. *Thaumarchaeota* are aerobic ammonia oxidizers (*21*), raising concerns that the TEX_{86} index can also reflect subsurface temperatures rather than a mixed-layer SST. However, available compound-specific carbon-isotope evidence indicates that the TEX_{86} temperature signal largely derives from the ocean mixed-layer (*22*). Using the current calibration [e.g., (*23*)], TEX_{86} tends to overestimate SSTs in the high latitudes and underestimate temperatures in the low latitudes (*24*). Indeed, TEX_{86} SSTs derived from surface sediments of the tropical Pacific show slightly lower temperature estimates than observed SSTs (see supplementary materials). Nevertheless, the late Pleistocene TEX_{86}-derived zonal SST gradient agrees with the modern gradient between sites 806 and 850 (supplementary materials) and broadly captures the temperature characteristics of these distinct regions. Finally, TEX_{86} temperature reconstructions can record much higher SSTs compared to the alkenone proxy (*25*), making it a more suitable proxy to evaluate the evolution of warm pool temperatures.

We reconstruct the history of equatorial Pacific temperature gradients for the past 12 million years using both TEX_{86} and $U^{K'}_{37}$ temperature proxies at ODP sites 769 (9°N, 121°E), 806, and 1143 (9°N, 113°E) in the western warm pool region and site 850 (1°N, 111°W) in the eastern Pacific cold tongue (Fig. 1). Our results illustrate a distinctly different thermal history of the Pacific warm pool compared to previously published records. For example, in contrast to relatively invariant Mg/Ca temperatures from site 806 (Fig. 2), TEX_{86} records from three localities near the center and edge of the modern warm pool unambiguously show ~4°C of cooling since the late Miocene (Fig. 3), with an ~2°C decline since the early Pliocene (Fig. 2). TEX_{86} values from the late Miocene to Pliocene also indicate that warm pool temperatures were almost always higher than the calculable limit of $U^{K'}_{37}$ temperatures until ~3-5 million years ago. Consequently, $U^{K'}_{37}$ temperatures cannot be applied to interpret the temperature history of the warm pool older than ~3 Ma (Figs. 2 and 3).

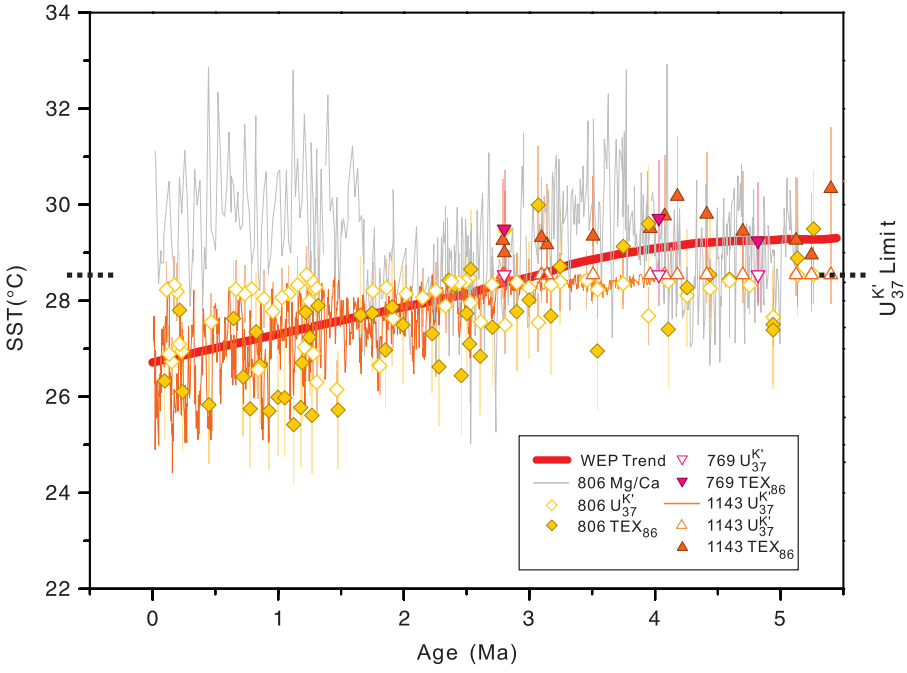

Fig. 2. SST reconstructions of the Pacific warm pool for the past 5 Ma. Mg/Ca temperatures do not account for changes in seawater Mg/Ca (*8*). Dashed line denotes the maximum calculable temperature (~28.5°C) of the $U^{K'}_{37}$ calibration. Calibration errors for $U^{K'}_{37}$ (*20*) and TEX_{86} (*23*) are 1.1° and 2.5°C, respectively, but vary spatially (*24*). Warm pool temperature trend is calculated with all TEX_{86}-derived SSTs and $U^{K'}_{37}$ temperatures after 3 Ma. $U^{K'}_{37}$- SST records from site 806 (5 to 0 Ma) (*4*) and 1143 (4 to 0 Ma) (*34*) are previously published.

Cold tongue $U^{K'}_{37}$ temperatures from site 850 in the western portion of the eastern equatorial upwelling region (Fig. 1) compare well with published alkenone records from sites 846 (*13*) and 847 (*12*) over the past 5 million years (Fig. 3). Site U1338 shows comparatively warmer temperatures (*26*), consistent with its location at the edge of the upwelling region (Fig. 1). Both TEX_{86} and $U^{K'}_{37}$ temperature reconstructions in the EEP region indicate that the cold tongue slowly cooled by ~6°C since 12 Ma, with higher cooling rates during the Pliocene and Pleistocene. TEX_{86} and $U^{K'}_{37}$ temperature estimates begin to deviate at about 6 Ma, with TEX_{86} SSTs showing consistently cooler temperatures, readily explained by differential changes in the depth and/or seasonality of production between haptophyte algae (alkenone producers) and archaea (supplementary materials). If changes in production depth are responsible for the temperature offset between these two proxies, production of archaea and haptophytes is still within the top 50 m of the mixed layer given the sharp vertical temperature gradient in the EEP (supplementary materials). Although sites 850 and U1338 represent the warmer edge of the EEP, alkenone values are still below the maximum temperature limit for 12 million years (Fig. 3)—in contrast to $U^{K'}_{37}$ temperatures in the western warm pool—and thus can record the cooling history of the EEP (Fig. 2 and supplementary materials).

We assess the evolution of the east-west equatorial Pacific temperature gradient (ΔT_{zonal}) by interpolating and averaging temperature results using TEX_{86} and $U^{K'}_{37}$ temperature records, and solely using TEX_{86} data (Fig. 4). Integrating all of the available SST data expands the spatial assessment for each region. However, because $U^{K'}_{37}$ is mostly maximized in warm pool samples older than 3 Ma, warm pool temperature reconstructions largely rest on TEX_{86} SST records prior to 3 Ma (Figs. 2 and 3). In contrast, the composite temperature of the cold tongue is dominated by $U^{K'}_{37}$ records (Figs. 2 and 3). At our localities, TEX_{86} values tend to yield lower temperature estimates than $U^{K'}_{37}$ when both are available (Figs. 2 and 3 and supplementary materials). As a result, our SST trends from the integrated data set often yield lower average temperatures in the warm pool, higher temperatures in the cold tongue, and a smaller ΔT_{zonal} relative to estimates that only use our TEX_{86} records (Fig. 4 and supplementary materials). For example, the Pliocene ΔT_{zonal} shows a range of 3.2°C (total data set) to 4.1°C (based solely on TEX_{86} data; see supplementary materials).

Averaging ΔT_{zonal} data over the Quaternary (2.6 to 0 Ma), Pliocene (5.3 to 2.6 Ma), and late Miocene (12 to 5.3 Ma) indicates that about 60 to 70% of the Quaternary ΔT_{zonal} is expressed in the late Miocene, whereas ~80% of the Quaternary ΔT_{zonal} characterizes the Pliocene and thus closely reflects modern oceanographic conditions (supplementary materials). Notably, our records indicate that both the warm pool and the cold tongue were warmer in the past, but that a cold EEP (relative

to the warm pool) was present. Thus, the oceanographic processes that produce the modern cold tongue, including a shallow EEP thermocline and active upwelling, were likely in play—consistent with high rates of biogenic opal accumulation in the EEP during the late Miocene and Pliocene (*27*).

A late Miocene–Pliocene climate state characterized by strong temperature asymmetry across the equatorial Pacific provides the necessary conditions for robust ENSO-type interannual climate variability but does not directly prove its existence. Regardless, our temperature reconstructions support other proxy records (*15*, *16*) and climate simulations (*28*, *29*) that indicate ENSO-like behavior during the Pliocene and beyond (*30*).

Today, waters of the Equatorial Undercurrent that source upwelled waters in the eastern equatorial Pacific derive from the extratropics and higher latitudes, including the Subantarctic mode water (*31*). Geochemical tracers, drifter experiments, and climate simulations (*32*) indicate that waters from the eastern, subtropical Pacific subduct and resurface in the EEP thermocline within two decades. Indeed, the linkage between the eastern equatorial Pacific and anomalously warm waters from higher latitudes was used to explain a period of prolonged warming of the EEP in the early 1990s (*32*). Similarly, during the late Miocene to Pliocene, warmer extratropical waters (*7*, *33*) (Fig. 4) that sourced the EEP likely contributed a reduction in ΔT_{zonal}. As meridional temperature gradients increased during global cooling, colder extratropical water contributed to EEP cooling and an increase in ΔT_{zonal} (Fig. 4).

Given the areal extent of tropical warm pools and their importance in regulating global temperatures, our new warm pool temperature records substantially revise the character and nature of global warming in the recent past.

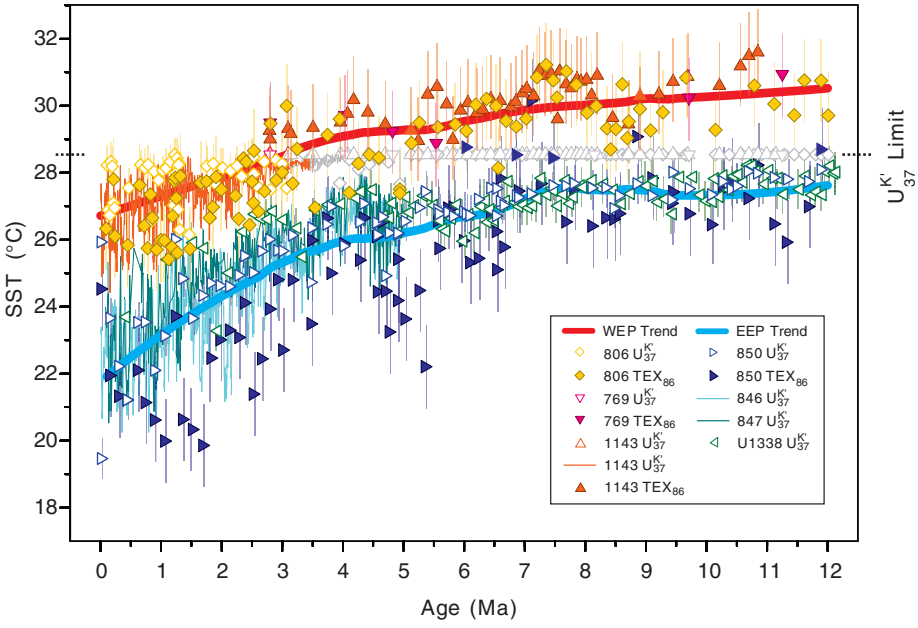

Fig. 3. Temperature evolution of the western and eastern equatorial Pacific since 12 Ma. All published data [$U^{K'}_{37}$ from sites 806 (5 to 0 Ma) (*4*); 846 (5 to 0 Ma) (*13*); 847 (5 to 0 Ma) (*12*); 1143 (4 to 0 Ma) (*34*); and U1338 (12 to 0 Ma) (*26*)] are converted to temperature with the calibration of Conte *et al*. (*20*) for $U^{K'}_{37}$ and Kim *et al*. (*23*) for TEX_{86}. Western equatorial Pacific (WEP) temperature trend is calculated with all TEX_{86} from sites 769, 806, and 1143. $U^{K'}_{37}$ records from ODP sites 806 and 1143 are also applied for the past 3 Ma. $U^{K'}_{37}$ data before 3 Ma, shown in gray, are mostly maximized and are not included in trend calculations. Temperature trend in the eastern equatorial Pacific (EEP) is calculated with $U^{K'}_{37}$ values from sites 846, 847, 850, and U1338 and with TEX_{86} results from site 850.

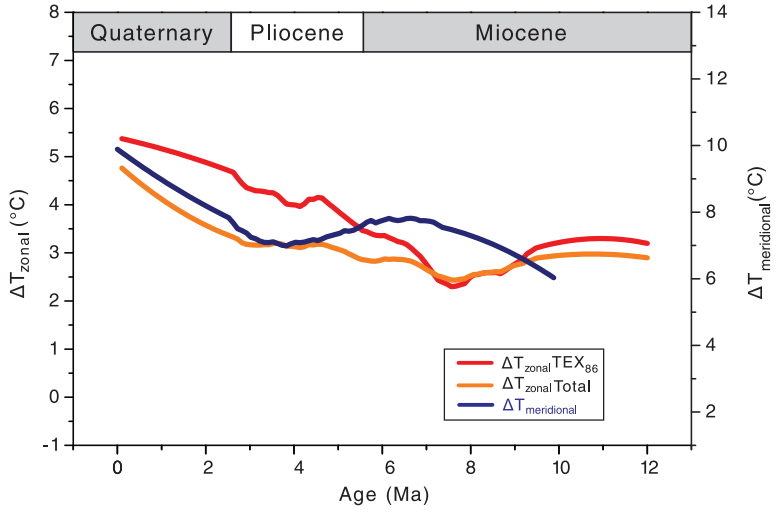

Fig. 4. Zonal (ΔT_{zonal}) and meridional ($\Delta T_{meridional}$) temperature gradients of the Pacific Ocean for the past 12 million years. Zonal gradient is computed with both $U^{K'}_{37}$ and TEX_{86} data, and with TEX_{86} data only. Meridional gradient is calculated between sites 806 and 1208 (*33*). Fifty-point Savitzky-Golay smoothing has been applied to the raw data. Note the different scales for ΔT_{zonal} and $\Delta T_{meridional}$.

References and Notes

1. M. J. McPhaden, S. E. Zebiak, M. H. Glantz, *Science* **314**, 1740–1745 (2006).
2. P. Molnar, M. A. Cane, *Paleoceanography* **17**, 11-1–11-11 (2002).
3. K. B. Karnauskas, R. Seager, A. Kaplan, Y. Kushnir, M. A. Cane, *J. Clim.* **22**, 4316–4321 (2009).
4. M. Pagani, Z. H. Liu, J. LaRiviere, A. C. Ravelo, *Nat. Geosci.* **3**, 27–30 (2010).
5. O. Seki *et al*., *Earth Planet. Sci. Lett.* **292**, 201–211 (2010).
6. D. J. Lunt *et al*., *Nat. Geosci.* **3**, 60–64 (2010).
7. C. M. Brierley *et al*., *Science* **323**, 1714–1718 (2009).
8. M. W. Wara, A. C. Ravelo, M. L. Delaney, *Science* **309**, 758–761 (2005).
9. V. Ramanathan, W. Collins, *Nature* **351**, 27–32 (1991).
10. I. N. Williams, R. T. Pierrehumbert, M. Huber, *Geophys. Res. Lett.* **36**, L21805 (2009).
11. M. Pagani, M. Huber, B. Sageman, in *Treatise on Geochemistry*, H. D. Holland, K. K. Turekian, Eds. (Elsevier, Oxford, 2014), pp. 281–304.
12. P. S. Dekens, A. C. Ravelo, M. D. McCarthy, *Paleoceanography* **22**, PA3211 (2007).
13. K. T. Lawrence, Z. Liu, T. D. Herbert, *Science* **312**, 79–83 (2006).
14. A. V. Fedorov *et al*., *Science* **312**, 1485–1489 (2006).
15. T. Watanabe *et al*., *Nature* **471**, 209–211 (2011).
16. N. Scroxton *et al*., *Paleoceanography* **26**, PA2215 (2011).
17. T. K. Lowenstein, M. N. Timofeeff, S. T. Brennan, L. A. Hardie, R. V. Demicco, *Science* **294**, 1086–1088 (2001).
18. R. M. Coggon, D. A. H. Teagle, C. E. Smith-Duque, J. C. Alt, M. J. Cooper, *Science* **327**, 1114–1117 (2010).
19. A. V. Fedorov *et al*., *Nature* **496**, 43–49 (2013).
20. M. Conte *et al*., *Geochem. Geophys. Geosyst.* **7**, Q02005 (2006).
21. M. Könneke *et al*., *Nature* **437**, 543–546 (2005).
22. S. G. Wakeham, C. M. Lewis, E. C. Hopmans, S. Schouten, J. S. Sinnighe Damsté, *Geochim. Cosmochim. Acta* **67**, 1359–1374 (2003).
23. J. H. Kim *et al*., *Geochim. Cosmochim. Acta* **74**, 4639–4654 (2010).
24. J. E. Tierney, M. P. Tingley, *Geochim. Cosmochim. Acta* **127**, 83–106 (2014).
25. S. Schouten, A. Forster, F. E. Panoto, J. S. Sinnighe Damste, *Org. Geochem.* **38**, 1537–1546 (2007).
26. G. Rousselle, C. Beltran, M.-A. Sicre, I. Raffi, M. De Rafelis, *Earth Planet. Sci. Lett.* **361**, 412–421 (2013).
27. J. W. Farrell *et al*., in *Proceedings of the Ocean Drilling Program, Scientific Results,* N. Pisias, L. Mayer, T. Janecek, A. Palmer-Julson, T. H. van Andel, Eds. (Ocean Drilling Program, College Station, TX, 1995), vol. 138.

28. A. M. Haywood, P. J. Valdes, V. L. Peck, *Paleoceanography* **22**, PA1213 (2007).
29. A. S. von der Heydt, A. Nnafie, H. A. Dijkstra, *Clim. Past* **7**, 903–915 (2011).
30. S. Galeotti *et al*., *Geology* **38**, 419–422 (2010).
31. J. R. Toggweiler, K. Dixon, W. S. Broecker, *J. Geophys. Res.* **96** (C11), 20467 (1991).
32. D. Gu, S. G. H. Philander, *Science* **275**, 805–807 (1997).
33. J. P. LaRiviere *et al*., *Nature* **486**, 97–100 (2012).
34. L. Li *et al*., *Earth Planet. Sci. Lett.* **309**, 10–20 (2011).

Acknowledgments: We thank M. Huber, H. Dijkstra, G. Foster, A. von der Heydt, M. Leckie, P. Hull, H. Spero, J. Zachos, A. Ravelo, A. Fedorov, and S. Hu for helpful discussions and four anonymous reviewers for their thoughtful reviews. This research used samples and data provided by the Integrated Ocean Drilling Program (IODP). Funding for this research was provided by NSF AGS 1203163 (to M.P.) and a Schlanger Ocean Drilling Fellowship (to Y.G.Z.), which is part of the NSF-sponsored U.S. Science Support Program for IODP that is administered by the Consortium for Ocean Leadership, Inc.

Supplementary Materials
www.sciencemag.org/content/344/6179/84/suppl/DC1
Materials and Methods
Figs. S1 to S7
Tables S1 to S4
References
Database S1

18 September 2013; accepted 14 February 2014
10.1126/science.1246172

Construction of a Vertebrate Embryo from Two Opposing Morphogen Gradients

Peng-Fei Xu,* Nathalie Houssin,* Karine F. Ferri-Lagneau,*† Bernard Thisse, Christine Thisse‡

Development of vertebrate embryos involves tightly regulated molecular and cellular processes that progressively instruct proliferating embryonic cells about their identity and behavior. Whereas numerous gene activities have been found to be essential during early embryogenesis, little is known about the minimal conditions and factors that would be sufficient to instruct pluripotent cells to organize the embryo. Here, we show that opposing gradients of bone morphogenetic protein (BMP) and Nodal, two transforming growth factor family members that act as morphogens, are sufficient to induce molecular and cellular mechanisms required to organize, in vivo or in vitro, uncommitted cells of the zebrafish blastula animal pole into a well-developed embryo.

The formation of vertebrate embryos depends on the activity of an organizing center, corresponding to the dorsal blastopore lip in amphibians and known as the Spemann-Mangold or dorsal organizer (*1*). When grafted ventrally into a host, this organizer results in the formation, at the site of the graft, of a secondary embryonic axis. The molecular nature of the activity carried by this dorsal tissue has been identified (*2*), and its main components are dorsally secreted factors that act as antagonists of ventral morphogens and help to establish a ventral-to-dorsal gradient of their activity (fig. S1A). However, when placed in a neutral environment such as the blastula animal pole, the Spemann organizer has very limited organizing activity, leading only to induction of axial mesendodermal tissues (*3*).

We previously established that, in zebrafish, the organizing activities controlling the development of the embryo are not restricted to the dorsal organizer but are distributed all along the embryonic margin (*3*, *4*) and result from the combined activity of two signaling pathways: bone morphogenetic protein (BMP) and Nodal. We found that the organizing activity of each portion of the embryonic margin varies depending on the BMP/Nodal ratio of activities (fig. S1B): A high BMP/Nodal ratio organizes the tail; a low BMP/Nodal ratio organizes the posterior head, whereas intermediate ratios of activity induce formation of the trunk (*4*). Based on these observations, we hypothesized that exposing uncommitted embryonic cells to a continuous variation of BMP/Nodal ratios may be sufficient to organize a complete embryonic axis (fig. S1C).

To test this hypothesis, we engineered opposing gradients of BMP and Nodal by injecting their corresponding mRNAs, at the 128-cell stage, into two different animal pole blastomeres that give rise to distinct clones of cells secreting these factors (Fig. 1A). The animal pole of the blastula was chosen as the territory to instruct because it contains all elements necessary to mediate the molecular and cellular responses to BMP and Nodal stimulation (*3*, *4*). Additionally, because the animal pole is distant from the margin, the influence of the primary axis and of maternal determinants is expected to be minimal.

In support of our hypothesis, these two secreting centers organize the animal pole cells (see supplementary materials and methods) into a secondary embryonic axis that forms at the animal pole (Fig. 1, B to E), solely from animal pole cells (fig. S2). These ectopic axes contain tissues and organs present in the primary axis and extend from the forebrain to the tip of the tail (Fig. 1B). In most cases, the primary and secondary axes fuse in the cephalic region, where animal pole cells are recruited by both growing structures. However, in some cases (1.3%; n = 1012 embryos), clones are in such a position that the two embryonic axes do not fuse (Fig. 1, C to E), with each displaying a forebrain, eyes, and a beating heart and exhibiting spontaneous myotomal contractions indicative of a functional nervous system (movie S1). Although the antero-posterior (A-P) axis of the primary embryo always parallels the animal-vegetal (An-Vg) axis of the egg, we found no correlation between the An-Vg axis of the egg and the A-P axis of the secondary embryo, which can be parallel, perpendicular, or even antiparallel to the A-P axis of the primary embryo and, therefore, to the An-Vg axis of the egg (Fig. 1, C to E). This demonstrates that, in zebrafish, there is no intrinsic information present in the egg or in the early embryo determining the orientation of the A-P axis that cannot be reversed by application of appropriate signals.

To understand the relative contribution of the two signaling pathways to the organization of the secondary embryonic axis, we examined the consequence of adding BMP or Nodal individually. At the blastula stage, BMP signaling is already active at the animal pole (*5*); adding more BMP to this region has very little effect (fig. S3). Conversely, at the blastula stage, stimulating the animal pole with Nodal results in a thickening of the animal pole blastoderm (Fig. 2A). At the onset of gastrulation, the central part of the resulting protrusion internalizes (Fig. 2, B and C), forming a blastopore with a circular, radially symmetrical blastopore lip where mesodermal cells involute (movie S2).

At blastula and gastrula stages, epiboly disperses cells of the animal pole over the ectoderm. However, in the presence of a Nodal-expressing clone, the surrounding animal pole cells do not spread but converge toward the center of the Nodal-secreting source (fig. S4). It is known that the guidance cues for convergence movements in the zebrafish gastrula are controlled by janus kinase/signal transducer and activator of transcription 3 (JAK/STAT3) signaling (*6*, *7*). Activation of STAT3 is independent of Nodal signaling but dependent on the maternal β-catenin signaling pathway (*6*). Because ectopic Nodal signaling induces an attracting center at the animal pole, we hypothesized that STAT3 may be activated in that domain. Consistent with this, in STAT3 morphant embryos, ectopic Nodal signaling fails to induce radial convergence movements, whereas internalization of the mesendoderm is not affected (Fig. 2D). Furthermore, Nodal induction of expression of *liv1* (Fig. 2E), a downstream target of STAT3 (*8*), is abolished in STAT3 morphant embryos (Fig. 2F), demonstrating that although Nodal is not required for activation of STAT3 in the dorsal domain of the blastula (*7*), it is sufficient to induce this activation at the animal pole.

In zebrafish, Nodal is known to be essential for inducing the organizing activity carried by the

Department of Cell Biology, University of Virginia, Charlottesville, VA 22908, USA.

*These authors contributed equally to this work.
†Present address: Biomedical/Biotechnology Research Institute, North Carolina Central University, Kannapolis, NC 28081, USA.
‡Corresponding author. E-mail: christhisse@virginia.edu